Young-Hoon Lee ; Hogun Jhang ; S. S. Kim ; Jungpyo Lee ✉

View Online   Export Citation   CrossMark

Articles You May Be Interested In

Stringer spin up due to anomalous transport

Physics of Plasmas (June 1998)

Metatranscriptomics workflow analysis from environmental sample of fungi

AIP Conference Proceedings (June 2016)

Physics of Plasmas

Features in Plasma Physics Webinars

Register Today!

AIP Publishing

Kinetic effects on geodesic acoustic modes and Stringer spin-up driven by a poloidally asymmetric particle source

View Online   Export Citation   CrossMark

Young-Hoon Lee,[1] (iD) Hogun Jhang,[2] (iD) S. S. Kim,[2] (iD) and Jungpyo Lee[1,a] (iD)

AFFILIATIONS

[1]Hanyang University, Department of Nuclear Engineering, Seoul 04763, South Korea
[2]Korea Institute of Fusion Energy, Daejon 34133, South Korea

[a]Author to whom correspondence should be addressed: jungpyo@hanyang.ac.kr

ABSTRACT

The impact of the poloidally inhomogeneous particle source on the onset of Stringer spin-up (SSU) and geodesic acoustic mode (GAM) is investigated. Using a gyrofluid model with Hammet–Perkins closure, it was found that Landau damping stabilizes both waves and subsequently makes a threshold. To capture the full effects of Landau damping, a gyrokinetic model is adopted and results are compared with those from the gyrofluid model. Both models predicted the same value of the threshold for SSU, while for the case of GAM, the gyrofluid model overestimates the threshold value. Considering maximal throughput of the ITER pellet fueling system, the source intensity is calculated at a similar or slightly lower level compared to the source threshold for SSU.

I. INTRODUCTION

A poloidally inhomogeneous particle source has been widely used in present-day tokamak experiments. Low or high field side pellet injection is used for either the replenishment of fuel ions[1–3] or the mitigation of edge localized modes (ELMs).[4,5] If the particle throughput is high enough to modify the plasma equilibrium, it may cause macroscopic magnetohydrodynamic (MHD) instabilities, which is believed to be the physics basis for the pellet pacemaking of ELMs. On the other hand, if the intensity of the inhomogeneous particle source is moderate, it may not cause an MHD instability but have an influence on plasma transport via generation of poloidal $\mathbf{E} \times \mathbf{B}$ flow.[6] The goal of this paper is to reexamine this $\mathbf{E} \times \mathbf{B}$ flow generation process by a poloidally inhomogeneous source while considering Landau damping and other kinetic effects.

It was first found by Stringer that poloidally inhomogeneous transport can drive a poloidal rotation.[7] This unstable poloidal rotation was named after him as Stringer spin-up (SSU) and further analyzed by Hassam and Drake.[8] It was found that an inhomogeneous particle source further destabilizes this process. This effect is useful to explain some experimental observations, such as the low to high (LH) mode transition[6] and the formation of the pellet enhanced performance (PEP) mode.[9] In addition to SSU, the inhomogeneous source can also destabilize the geodesic acoustic mode (GAM). In tokamak

plasmas, the presence of $\mathbf{E} \times \mathbf{B}$ compressibility due to a temporally fast variation coupled with geodesic curvature can drive GAMs.[10–12] Early studies on GAM generation concentrated on the turbulence driven process,[11,13,14] while more recent studies reported the GAM excitation during a nonlinear pedestal collapse[15] and the parametric process.[16,17] However, we do not consider turbulence or any other nonlinear and kinetic drive but only the poloidally asymmetric particle source driven GAM in this paper.

In realistic tokamak geometry, poloidal rotation and GAMs, once generated, are subject to damping via various physical processes. In a short ion transit time scale, the transit time magnetic pumping prevails,[18,19] while the ion–ion collision governs the eventual damping in a long time scale when $t > \varepsilon \tau_{ii}$ (ε: inverse aspect ratio, τ_{ii}: ion–ion collision time).[20] In particular, the Landau damping representing the parallel phase mixing will have influence on the $\mathbf{E} \times \mathbf{B}$ flow generation by the source because its time scale may well be relevant to that in dynamics involved (i.e., $1/\omega_{ti} \ll 1/\gamma_{LD} \ll \tau_D$, where γ_{LD} is the Landau damping rate[21–23] and τ_D is the parallel particle relaxation time). Therefore, one may expect that the Landau damping should have an impact on the efficacy of the $\mathbf{E} \times \mathbf{B}$ flow generation by a poloidally inhomogeneous particle source. Therefore, the focus of this paper is to extend the theory of the source induced SSU and GAM, with a special emphasis on the impact of the Landau damping. This requires

an extension of the original reduced MHD model (rMHD)[8] to capture the physics of the Landau damping, which is the main motivation for us to utilize either gyro-Landau fluid 4-moment (GLF4M) or gyrokinetic (GK) model.

In the GLF4M model, a closure model of Hammet–Perkins[24] is implemented in order to reproduce the Landau damping. As will be shown in Sec. III, compared to the rMHD model, the GLF4M model exhibits a threshold source intensity beyond which either GAM or SSU becomes destabilized. It is because the Landau damping gives significant attenuation to both waves. Next, having demonstrated that Landau damping is key to threshold physics, the GK model is additionally adopted in Sec. IV for the exact calculation of the threshold. The effect of Landau damping can be fully captured in GK dispersion relation by using plasma dispersion functions. By comparing results with GLF4M and GK models, it was found that both models give the same evaluation to the threshold of SSU; however, for the case of GAM, some deviations between them is shown.

The scope of this paper is restricted to the initial growing phase of an unstable mode from an equilibrium condition. If a poloidally asymmetric particle source is once injected, an equilibrium flow is generated to prevent particles to be accumulated in one direction on the poloidal coordinate. All the simulations and dispersion relations are conducted and derived on this well-established equilibrium condition. The saturation and final damping of the $\mathbf{E} \times \mathbf{B}$ flow require other physics elements, such as the residual zonal flow[20,25] and collisional damping,[18,19,26] which is outside of scope of this paper.

The rest of this paper is organized as follows. The rMHD model by Hassam, which describes unstable $\mathbf{E} \times \mathbf{B}$ flow driven by a poloidally asymmetric source, is briefly reviewed in Sec. II. In Sec. III, the GLF4M model equations are presented and the dispersion relation is derived. Comparing numerical results between the GLF4M model and the rMHD model, the distinguishing features of the GLF4M model are highlighted, while equivalence between the two models is also demonstrated in Appendix C. In Sec. IV, the GK model is presented and the dispersion relation is also derived using a plasma dispersion function. Parameter scans of the source threshold are conducted using the GK and GLF4M dispersion relations. Finally, we conclude this paper in Sec. V with a summary of the main results and some discussions with the practical example of ITER pellet injection system.

II. REDUCED MHD DESCRIPTION

A. Equations

In this section, we briefly review the rMHD that has been used in Ref. 8 for a study of a poloidally inhomogeneous source driven instability. This consists of the conservation equations for the density n and the fluid velocity $\mathbf{u}$,

$$\frac{\partial n}{\partial t} + \nabla \cdot n\mathbf{u}_\perp + \mathbf{B} \cdot \nabla\left(\frac{n u_\parallel}{B}\right) = S, \tag{1}$$

$$n m_i\left(\frac{\partial \mathbf{u}}{\partial t} + \mathbf{u} \cdot \nabla \mathbf{u}\right) = -\nabla p + \mathbf{J} \times \mathbf{B} - m_i S\mathbf{u}, \tag{2}$$

together with the quasi-neutrality condition

$$\nabla \cdot \mathbf{J} = 0 \tag{3}$$

and the ideal Ohm's law $\mathbf{E} + \mathbf{u} \times \mathbf{B} = 0$. Here, $p = nT$ is the pressure, $\mathbf{J}$ is the current density, $\mathbf{E}$ is the electric field, and $S = S(r, \theta)$ is a

particle source with r and θ the radial and poloidal coordinates, respectively. A concentric circular equilibrium is considered here. Note that there is no momentum source but only particle one in this model. The last term in Eq. (2) arises from the relation $\frac{\partial n\mathbf{u}}{\partial t} + \nabla \cdot (n\mathbf{u}\mathbf{u}) = n\left(\frac{\partial \mathbf{u}}{\partial t} + \mathbf{u}\nabla \cdot \mathbf{u}\right) + \mathbf{u}\left(\frac{\partial n}{\partial t} + \nabla \cdot (n\mathbf{u})\right)$ together with Eq. (1). The equation for the parallel velocity $u_\parallel$ is obtained by taking a scalar product with $\mathbf{b} = \mathbf{B}/|\mathbf{B}|$ on both sides of Eq. (2),

$$\frac{\partial u_\parallel}{\partial t} + \mathbf{b}\mathbf{u} : \nabla \mathbf{u} = -v_{T_i}^2 \nabla_\parallel \ln n - \frac{S}{n} u_\parallel, \tag{4}$$

where $v_{T_i} = \sqrt{T/m_i}$ is the ion thermal velocity, $\nabla_\parallel \simeq (qR_0)^{-1}\partial/\partial\theta$ is the derivative along the parallel direction, $q \equiv rB_0/(R_0 B_p)$ is the safety factor, and R_0 is the major radius. The parallel temperature gradient is assumed to be negligibly small, and isothermal plasmas between species are assumed. The vorticity equation for the $\mathbf{E} \times \mathbf{B}$ velocity is obtained by taking a scalar product with $R^2\mathbf{B}_p$ on Eq. (2) and applying the quasi-neutrality condition. Then, it is represented by an integral form on a given flux-surface average,

$$\oint \frac{d\theta}{\mathbf{B} \cdot \nabla\theta} R^2\mathbf{B}_\mathbf{p} \cdot \left(n m_i \frac{d\mathbf{u}}{dt} + T\nabla n\right) = 0, \tag{5}$$

where $d/dt = \partial/\partial t + \mathbf{u} \cdot \nabla$ is a convective derivative and $\mathbf{B}_\mathbf{p}$ is the poloidal magnetic field. Now, from Eqs. (1), (4), and (5), one can derive a set of reduced equations by expanding them in terms of the inverse aspect ratio $\varepsilon \equiv r/R_0$, which is assumed to be small by considering a high aspect ratio tokamak. After expansion, equations can be further simplified by separating them into the poloidally averaged part and the varying one [i.e., $f(r, \theta) = \bar{f}(r) + \tilde{f}(r, \theta)$]. The linearized equations for normalized density $\tilde{N} \equiv n_1/n_0$, parallel velocity $\tilde{u}_\parallel$, and $\mathbf{E} \times \mathbf{B}$ velocity u_E are then given by

$$\frac{\partial \tilde{N}}{\partial t} + \frac{u_E}{r}\frac{\partial \tilde{N}}{\partial \theta} - 2\varepsilon \frac{u_E}{r}\sin\theta + \nabla_\parallel \tilde{u}_\parallel = \frac{\tilde{S}}{n_0}, \tag{6}$$

$$\frac{\partial \tilde{u}_\parallel}{\partial t} + \frac{u_E}{r}\frac{\partial \tilde{u}_\parallel}{\partial \theta} = -v_{T_i}^2 \nabla_\parallel \tilde{N}, \tag{7}$$

$$\frac{\partial u_E}{\partial t} = -\frac{2\varepsilon v_{T_i}^2}{r}\oint\left(\frac{d\theta}{2\pi}\right)\tilde{N}\sin\theta, \tag{8}$$

where n_0 and n_1 are the averaged and perturbed density, respectively. The set of reduced Eqs. (6)–(8) can describe not only SSU but also GAM driven by a poloidally inhomogeneous source.

B. Dispersion relation

Since we focus on the initial growing phase of the perturbation, we first set an equilibrium condition following Ref. 8 and consider how the initial perturbation evolves. The equilibrium condition can be simply derived by assuming a steady-state without any perturbation ($u_E = 0$), giving rise to

$$\nabla_\parallel \tilde{u}_\parallel^{Eq} = \frac{\tilde{S}}{n_0}, \tag{9}$$

$$\nabla_\parallel \tilde{N}^{Eq} = 0, \tag{10}$$

where the superscript "Eq" means an equilibrium quantity. From Eq. (9), one finds that a parallel equilibrium flow is established as

$$\tilde{u}_{\parallel}^{Eq} = qR_0 \int d\theta \, \frac{\tilde{S}}{n_0}, \tag{11}$$

which balances out the poloidally inhomogeneous particle source. Then, for a small perturbation from the equilibrium, a dispersion relation can be derived in the form of

$$\hat{\omega}\left[\hat{\omega}^2 - (1 + 2q^2)\right] + i\frac{q^2}{\varepsilon}\hat{S}_c = 0. \tag{12}$$

Here, $\hat{\omega} \equiv \omega/\omega_{ti}$ is the normalized frequency with the transit frequency for thermal ions $\omega_{ti} = v_{T_i}/qR_0$ and $\hat{S}_c \equiv \tilde{S}_c/n_0\omega_{ti}$ is a normalized in-out asymmetric source intensity. The subscripts s and c denote the Fourier coefficients of its $\sin\theta$ and $\cos\theta$ components, respectively. The detailed derivation can be found in Ref. 8. From Eq. (12), note that SSU is destabilized in the case of an outboard source ($\hat{S}_c > 0$), while GAM becomes unstable in the case of an inboard source ($\hat{S}_c < 0$). If there is no poloidally asymmetric source ($\hat{S}_c = 0$), marginally stable GAM is derived as $\omega_{GAM}^{rMHD} = \sqrt{1 + 2q^2}\,\omega_{ti}$. One notable point here is that an up–down asymmetric source ($\hat{S} \propto \sin\theta$) does not cause these source-driven modes.

A time evolution of the $\mathbf{E} \times \mathbf{B}$ flow obtained by numerically solving rMHD Eqs. (6)–(8) when $\varepsilon = 0.1$ and $q = 1.4$ is shown in Fig. 1. In this computation, a normalized poloidal source is used with various intensities, and the initial condition is set by the equilibrium condition shown in Eqs. (9)–(11) while allowing a little perturbation to the initial $\mathbf{E} \times \mathbf{B}$ flow. The results with an outboard source $\hat{S}_c = 0.05$ and an inboard one $\hat{S}_c = -0.05$ are plotted in Figs. 1(a) and 1(b), respectively, while one without any poloidal source $\hat{S}_c = 0.00$ is depicted in Fig. 1(c). As expected from the rMHD dispersion relation, SSU (GAM) becomes unstable with an outboard (inboard) source. A non-growing GAM, however, is observed without any poloidal source. Here, note that there is no threshold of the source intensity to destabilize SSU or GAM in either cases of outboard and inboard sources. It is because the rMHD model excludes any kinetic effects that brings about significant damping to the wave. In Secs. III and IV, the kinetic effect, especially the ion Landau damping, will be included by employing a closure to the fluid model (Sec. III) or by a full kinetic model (Sec. IV).

III. GYROFLUID DESCRIPTION

In this section, we study the poloidal source-driven instability using a gyro-Landau fluid 4-moment (GLF4M) model. We follow the procedure developed by Beer and Hammet[27–29] to obtain a set of GLF4M equations from an appropriate gyrokinetic (GK) equation. Although the Beer–Hammet GLF model focused on a study of drift wave type micro-turbulence, our focus is in studying the meso-scale instability whose characteristic scale length is set by that of the poloidally asymmetric source [i.e., $k_\perp \rho_i \sim \mathcal{O}(\varepsilon)$, where $k_\perp$ is the perpendicular wave number and ρ_i is the ion Larmor radius]. Since poloidally inhomogeneous sources usually have low poloidal mode number m due to their slow parallel variation (i.e., $m = 0, \pm 1, \pm 2, \ldots$ are small), one can assume that the poloidal source has a zonal-like structure [i.e., $n = 0, m \simeq 0$, but $k_r\rho_i \sim \mathcal{O}(\varepsilon)$, where n is the toroidal mode number]. Therefore, one can neglect terms that are proportional to the diamagnetic frequency $i\omega_* \equiv -(T/eBn_0)\nabla n_0 \cdot \hat{\mathbf{b}} \times \nabla \propto k_\theta\rho_i$, which usually play a role as a driver of drift wave-type instabilities, such as ion temperature gradient modes (ITG) or trapped electron modes (TEM). To summarize before deriving GLF4M equations, physics of the meso-scale source driven instability is isolated from that of micro-scale
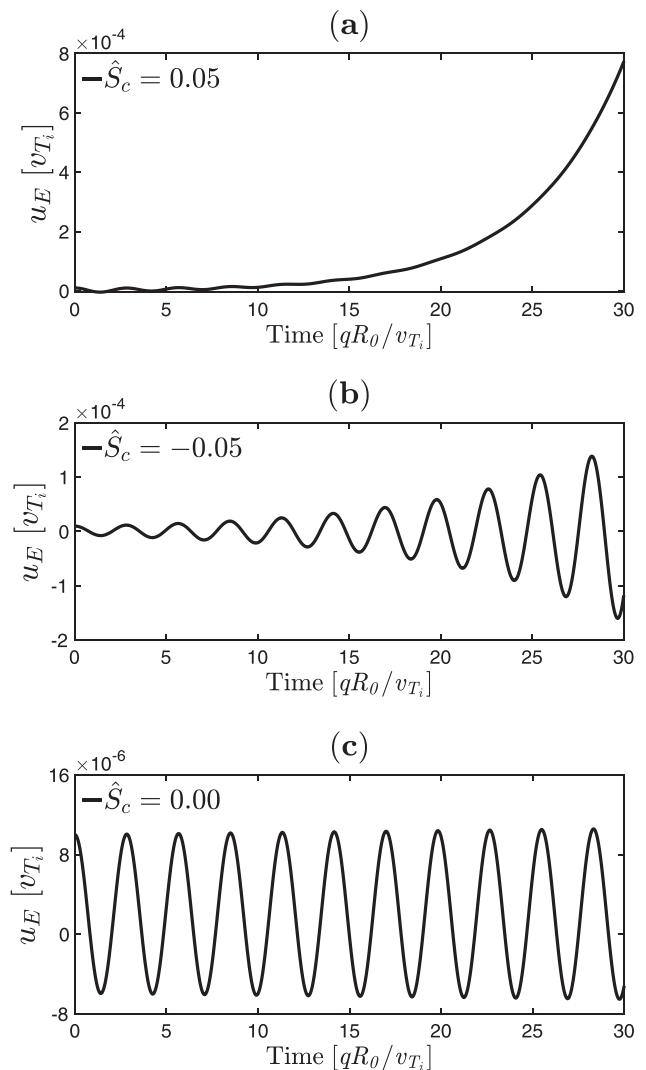

FIG. 1. Time evolution of the $\mathbf{E} \times \mathbf{B}$ flow in the rMHD model when $(\varepsilon, q) = (0.1, 1.4)$. Results with outboard $\hat{S}_c = 0.05$ and inboard sources $\hat{S}_c = 0.05$ are shown in (a) and (b), respectively. Shown in (c) is when $\hat{S}_c = 0.00$.

turbulence assuming that the poloidal source has a zonal-like structure and there is no nonlinear interaction between them in our study.

A. Equations

The collisionless GK equation for the zonal component with the perpendicular wavenumber vector $\mathbf{k}_\perp \simeq k_r\nabla r$ is given in terms of the perturbed gyro-center distribution function $\delta f_{\mathbf{k}_\perp}^{(g)}$ by

$$\left(\frac{\partial}{\partial t} + \mathbf{v}_E \cdot \nabla + v_{\parallel}\mathbf{b} \cdot \nabla + i\omega_D\right)\delta f_{\mathbf{k}_\perp}^{(g)}$$

$$= -\left(v_{\parallel}\mathbf{b} \cdot \nabla + i\omega_D\right)\left(F_0 J_0 \frac{e\phi_{\mathbf{k}_\perp}}{T}\right) + S_{\mathbf{k}_\perp}F_0, \tag{13}$$

where F_0 is an equilibrium distribution function taking the Maxwellian form, $J_0 = J_0(k_\perp\rho)$ is the zeroth-order Bessel function,

$\rho \equiv v_\perp/\Omega$ is the gyroradius with the gyrofrequency $\Omega \equiv eB_0/(mc)$, and $\mathbf{v}_E \equiv (\mathbf{b} \times \nabla J_0 \phi_{k_\perp})/B_0$ is the gyroaveraged $\mathbf{E} \times \mathbf{B}$ drift. The drift frequency ω_D due to ∇B and curvature is defined as $i\omega_D = (\frac{v_\parallel^2 + v_\perp^2/2}{\Omega B^2})\mathbf{B} \times \nabla B \cdot \nabla$. Here, the subscript representing the particle species is omitted for simplicity. The perturbed gyrocenter distribution function $\delta f_{k_\perp}^{(g)}$ consists of adiabatic and non-adiabatic parts [i.e., $\delta f_{k_\perp}^{(g)} = -F_0 J_0 (e\phi_{k_\perp}/T) + g_{k_\perp}$]. The electrostatic potential $\phi_{k_\perp}$ is determined by the Poisson equation

$$\left(\left\langle J_0 \hat{\delta f}_{ik_\perp}^{(g)} \right\rangle - n_0 \frac{e\phi_{k_\perp}}{T_i}[1 - \Gamma(b_i)] \right)$$
$$- \left(\left\langle J_0 \hat{\delta f}_{ek_\perp}^{(g)} \right\rangle + n_0 \frac{e\phi_{k_\perp}}{T_e}[1 - \Gamma(b_e)] \right) = n_0 \frac{e\phi_{k_\perp}}{T_e}(k_\perp \lambda_{De})^2$$

(14)

using a velocity-integral $\langle A \rangle \equiv [\int d^3v F_0 A]/[\int d^3v F_0] = [2\pi \times \int\int v_\perp dv_\perp dv_\parallel]/n$. Here, $\hat{f}_{ik_\perp}^{(g)} \equiv f_{ik_\perp}^{(g)}/F_0$ is the gyrocenter distribution function normalized to the equilibrium one, $\lambda_{De} = \sqrt{T_e/(4\pi e^2 n_0)}$ is the electron Debye length, $b_s = (k_r \rho_{ts})^2$ with $\rho_{ts} = v_{T_s}/\Omega_s$, and $\Gamma(b_s) = I_0(b_s)e^{-b_s}$ with I_0 denoting the zeroth-order modified Bessel function.

By taking velocity moments of Eq. (13), one can derive a set of gyrofluid equations as

$$\frac{\partial \delta n_{k_\perp}}{\partial t} + \mathbf{u}_E \cdot \nabla \delta n_{k_\perp} + \mathbf{B} \cdot \nabla \frac{n_0 u_{\parallel k_\perp}}{B} + i\omega_D \left(\frac{\delta p_{\parallel k_\perp} + \delta p_{\perp k_\perp}}{T} \right)$$
$$= -\left(2 + \frac{1}{2}\hat{\nabla}_\perp^2\right) i\omega_D \frac{e\phi_{k_\perp}}{T} e^{-b/2} + S_{k_\perp}^{\delta n},$$

(15a)

$$mn_0 \frac{\partial u_{\parallel k_\perp}}{\partial t} + \mathbf{u}_E \cdot \nabla u_{\parallel k_\perp} + \mathbf{B} \cdot \nabla \frac{\delta p_{\parallel k_\perp}}{B}$$
$$+ \delta p_{\perp k_\perp} \nabla_\parallel \ln B + i\omega_D \left(\frac{q_{\parallel k_\perp} + q_{\perp k_\perp} + 4p_0 u_{\parallel k_\perp}}{T/m} \right)$$
$$= -n_0 e \left(\mathbf{B} \cdot \nabla \frac{\phi_{k_\perp}}{B} e^{-b/2} + \frac{1}{2}\hat{\nabla}_\perp^2 \phi_{k_\perp} e^{-b/2} \nabla_\parallel \ln B \right) + S_{k_\perp}^{u\parallel},$$

(15b)

$$\frac{\partial \delta p_{\parallel k_\perp}}{\partial t} + \mathbf{u}_E \cdot \nabla \delta p_{\parallel k_\perp} + \mathbf{B} \cdot \nabla \left(\frac{q_{\parallel k_\perp} + 3p_0 u_{\parallel k_\perp}}{B} \right)$$
$$+ 2(q_{\parallel k_\perp} + 3p_0 u_{\parallel k_\perp}) \nabla_\parallel \ln B + i\omega_D \left(\frac{\delta r_{\parallel, \parallel k_\perp} + \delta r_{\parallel, \perp k_\perp}}{T/m} \right)$$
$$= -\left(4 + \frac{1}{2}\hat{\nabla}_\perp^2\right) i\omega_D p_0 \frac{e\phi_{k_\perp}}{T} e^{-b/2} + S_{k_\perp}^{\delta p\parallel},$$

(15c)

$$\frac{\partial \delta p_{\perp k_\perp}}{\partial t} + \mathbf{u}_E \cdot \nabla \delta p_{\perp k_\perp} + \mathbf{B} \cdot \nabla \left(\frac{q_{\perp k_\perp} + p_0 u_{\parallel k_\perp}}{B} \right)$$
$$- (q_{\perp k_\perp} + p_0 u_{\parallel k_\perp}) \nabla_\parallel \ln B + i\omega_D \left(\frac{\delta r_{\parallel, \perp k_\perp} + \delta r_{\perp, \perp k_\perp}}{T/m} \right)$$
$$= -\left(3 + \frac{3}{2}\hat{\nabla}_\perp^2 + \hat{\hat{\nabla}}_\perp^2\right) i\omega_D p_0 \frac{e\phi_{k_\perp}}{T} e^{-b/2} + S_{k_\perp}^{\delta p\perp},$$

(15d)

where $(e\phi_{k_\perp}/T)e^{-b/2}$ represents the gyroaveraged potential by using the approximation $\langle J_0 \rangle \simeq e^{-b/2}$. Here, definitions of all the fluid

variables $[\delta n_{k_\perp}, n_0 u_{\parallel k_\perp}, \delta p_{\parallel k_\perp}, \delta p_{\perp k_\perp}]$, $[S_{k_\perp}^{\delta n}, S_{k_\perp}^{u\parallel}, S_{k_\perp}^{\delta p\parallel}, S_{k_\perp}^{\delta p\perp}]$, $[q_{\parallel k_\perp}, q_{\perp k_\perp}]$, and $[\delta r_{\parallel, \parallel k_\perp}, \delta r_{\parallel, \perp k_\perp}, \delta r_{\perp, \perp k_\perp}]$ and the gyroaveraging operators $[\hat{\nabla}_\perp^2, \hat{\hat{\nabla}}_\perp^2]$ are defined in Appendix A for conciseness. Note that Eqs. (15a)–(15d) all contain nonlinear $\mathbf{E} \times \mathbf{B}$ convective terms represented by $\mathbf{u}_E \cdot \nabla(\cdots)$. Here, $\mathbf{u}_E = B^{-1}\mathbf{b} \times \nabla \phi_{k_\perp} e^{-b/2}$ is the gyro-averaged $\mathbf{E} \times \mathbf{B}$ flow, which can be approximated as $\mathbf{u}_E \simeq (ik_r/B)\phi_{k_\perp} e^{-b/2}\mathbf{e}_\theta$ with $\mathbf{e}_\theta$ the unit vector along the poloidal direction. Finally, considering the wavenumber region of $k_r \rho_{ti} < 1$, the quasi-neutrality condition with an adiabatic electron response $\delta n_{e k_\perp} = n_0 e(\phi_{k_\perp} - \langle\phi_{k_\perp}\rangle_\psi)/T_e$ is given by

$$e^{-b_i/2}\left(\frac{\delta n_{k_\perp}}{n_0} - \frac{b_i}{2}\frac{\delta T_{\perp k_\perp}}{T_i} \right) - [1 - \Gamma_0(b_i)]\frac{e\phi_{k_\perp}}{T_i} = \frac{e}{T_e}\left(\phi_{k_\perp} - \langle\phi_{k_\perp}\rangle_\psi \right),$$

(16)

where $\langle A \rangle_\psi \equiv [\oint d\theta(\mathbf{B}\cdot\nabla\theta)^{-1}A]/[\oint d\theta(\mathbf{B}\cdot\nabla\theta)^{-1}]$ is a flux-surface-average (FSA) of A.

B. Closure model

Closure models for the third-order $[q_{\parallel k_\perp}, q_{\perp k_\perp}]$ and the fourth-order $[\delta r_{\parallel, \parallel k_\perp}, \delta r_{\parallel, \perp k_\perp}, \delta r_{\perp, \perp k_\perp}]$ fluid variables are necessary to close the set of Eqs. (15a)–(15d). For the third-order variables, we take the Hammet–Perkins type closure[24] that has been devised to reproduce the linear Landau damping. The closures implemented in this work are represented by

$$[q_{\parallel k_\perp m}, q_{\perp k_\perp m}] = -i\chi \frac{m}{|m|} n_0 v_{T_i} [2\delta T_{\parallel k_\perp m}, \delta T_{\perp k_\perp m}],$$

(17)

where "m" is the poloidal mode number and the perturbed parallel and perpendicular temperatures are determined by the linear relation $[\delta T_{\parallel k_\perp}, \delta T_{\perp k_\perp}] = ([\delta p_{\parallel k_\perp}, \delta p_{\perp k_\perp}] - T\delta n_{k_\perp})/n_0$. Here, the coefficient χ has been evaluated as $\sqrt{2/\pi}$ by matching the fluid response function to the kinetic one in the low frequency limit $(qR_0\omega)/v_{T_i} \ll 1$. Although the GAM oscillations is found to have frequency of $\omega_{GAM} \propto v_{T_i}/R_0$, the closure gives good approximation to the local kinetic response even in the high frequency limit $(qR_0\omega)/v_{T_i} \gg 1$. It can be inferred that it is because the closure is used in fluid equations. For the fourth-order variables, we use simple Maxwellian closures[29] for long-time evolution, which means that perturbed parallel and perpendicular temperatures are ignored due to the short-time phenomena, the Landau damping

$$[\delta r_{\parallel, \parallel k_\perp}, \delta r_{\parallel, \perp k_\perp}, \delta r_{\perp, \perp k_\perp}] = v_{T_i}^2 T\delta n_{k_\perp}[3, 1, 2].$$

(18)

Finally, the GLF4M model including an inhomogeneous poloidal source is derived. It is composed of four-moment gyrofluid Eqs. (15a)–(15d), the quasi-neutrality condition Eq. (16), and closure models for the third- and fourth-order fluid variables Eqs. (17) and (18).

C. Dispersion relation

As done in Sec. II B, the equilibrium condition corresponding to the GLF4M model can be derived by assuming a steady-state in Eqs. (15a)–(15d) without any perturbation $\mathbf{u}_E = 0$. They correspond to

$$\mathbf{B} \cdot \nabla \frac{n_0 \tilde{u}_{\parallel k_\perp}^{Eq}}{B} = \tilde{S}_{k_\perp}^{\delta n},$$

(19a)

$$\mathbf{B} \cdot \nabla \left(\frac{\tilde{q}_{\parallel \mathbf{k}_\perp}^{Eq} + 3 p_0 \tilde{u}_{\parallel \mathbf{k}_\perp}^{Eq}}{B} \right) = 0, \tag{19b}$$

$$\mathbf{B} \cdot \nabla \left(\frac{\tilde{q}_{\perp \mathbf{k}_\perp}^{Eq} + p_0 \tilde{u}_{\parallel \mathbf{k}_\perp}^{Eq}}{B} \right) = 0. \tag{19c}$$

From Eq. (19a), a parallel equilibrium flow is generated when one neglects small terms of order $\mathcal{O}(\varepsilon)$. In addition, parallel and perpendicular heat flows are also generated from Eqs. (19b) and (19c) to satisfy the equilibrium of Eqs. (15c) and (15d). These corresponding equilibrium particle and heat flows are given in the form of

$$\tilde{u}_{\parallel \mathbf{k}_\perp}^{Eq} = q R_0 \int d\theta \, \frac{\tilde{S}_{\mathbf{k}_\perp}^{\delta n}}{n_0}, \tag{20a}$$

$$\tilde{q}_{\parallel \mathbf{k}_\perp m}^{Eq} = -3 p_0 \tilde{u}_{\parallel \mathbf{k}_\perp m}^{Eq}, \tag{20b}$$

$$\tilde{q}_{\perp \mathbf{k}_\perp m}^{Eq} = -p_0 \tilde{u}_{\parallel \mathbf{k}_\perp m}^{Eq}. \tag{20c}$$

To make an analytic interpretation, we only consider dominant poloidal mode components $m = 0, \pm 1$ of Eqs. (15a)–(15d) and apply a little $\mathbf{E} \times \mathbf{B}$ perturbation from pre-described equilibrium conditions. Then, one can derive a linear dispersion relation for the perturbation, which is given in the form of

$$c_5 \hat{\omega}^5 + c_4 \hat{\omega}^4 + c_3 \hat{\omega}^3 + c_2 \hat{\omega}^2 + c_1 \hat{\omega}^1 + c_0 = 0, \tag{21}$$

where the coefficients c_n ($n = 0, 1, \ldots, 5$) are given in Eq. (B17). By considering Eq. (B26), one can find that only an in-out asymmetric source affects the source-driven modes, which is consistent with the rMHD dispersion relation shown in Eq. (12). However, because isothermality between species is not assumed and the Hammet–Perkins closure is adopted in the GLF4M model, effects of temperature ratio between species and Landau damping influence the dispersion relation via the coefficients $\tau_e \equiv T_e/T_i$ and χ. It is also worth noting that the dispersion relation obtained from the GLF4M model is exactly reduced to that from the rMHD model under certain limit [i.e., when $\delta n_{e \mathbf{k}_\perp} = 0$ and $\chi \to \infty$, Eq. (21) becomes Eq. (12)]. This is because the quasi-neutrality condition Eq. (16) in the GLF4M model is equivalent to the vorticity Eq. (8) in the rMHD model. The equivalence between Eqs. (16) and (8) is demonstrated in Appendix C with an appropriate limit.

A time evolution of the $\mathbf{E} \times \mathbf{B}$ flow obtained by numerically solving GLF4M Eqs. (15a)–(15d) when $\varepsilon = 0.1$, $q = 1.4$, and $\tau_e = 1.0$ is shown in Fig. 2. In the simulation, the normalized poloidal source $\hat{S}_c \equiv S_{\mathbf{k}_\perp}^{\delta n}/(n_0 \omega_{ti})$ is used with various intensities and the initial condition is set by the equilibrium condition shown in Eqs. (19) and (20) while allowing a small perturbation to the initial $\mathbf{E} \times \mathbf{B}$ flow. The results with outboard sources $\hat{S}_c = 0.05$ and 0.15 are plotted with dotted and solid curves in Fig. 2(a), respectively, while those with inboard sources $\hat{S}_c = -0.05$ and -0.15 are also shown with dotted and solid curves in Fig. 2(b), respectively. For the outboard source case shown in Fig. 2(a), the initial damping of GAM occurs regardless of the source intensity (cf. the oscillatory damping feature when Time $\lesssim 5 \, [q R_0/v_{T_i}]$). By comparing with the damping of GAM for the case with the less intense source $\hat{S}_c = 0.05$ (dotted), the unstable SSU appears when a more intense source $\hat{S}_c = 0.15$ (solid) is applied, indicating an existence of source threshold for SSU between $\hat{S}_c = 0.05$
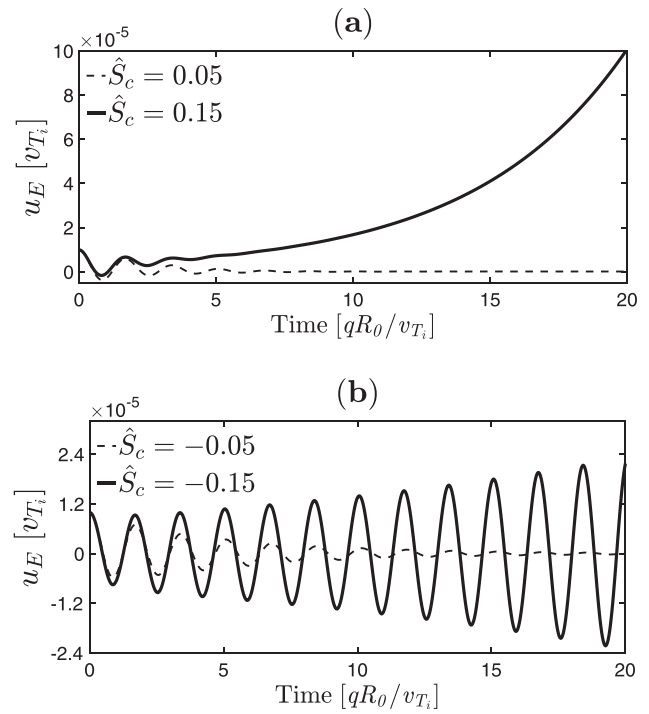

FIG. 2. Time evolution of the $\mathbf{E} \times \mathbf{B}$ flow in the GLF4M model when $(\varepsilon, q, \tau_e) = (0.1, 1.4, 1.0)$. Results with outboard sources $\hat{S}_c = 0.05$ (dotted) and $\hat{S}_c = 0.15$ (solid) are shown in (a), while those with inboard sources $\hat{S}_c = -0.05$ (dotted) and $\hat{S}_c = -0.15$ (solid) are shown in (b).

and $\hat{S}_c = 0.15$. On the other hand, as shown in Fig. 2(b), GAM is destabilized by the inboard source as shown with the result for $\hat{S}_c = -0.15$ (solid), while it is Landau damped out when the source is weak as shown with the result for $\hat{S}_c = -0.05$ (dotted). In other words, there exists the threshold source intensity in both cases. However, each case has a different type of unstable mode; unstable SSU for the outboard source and unstable GAM for the inboard one. Thus, the existence of the source threshold is revealed with the GLF4M model because it retains the effect of Landau damping. However, the effect of Landau damping actually originates from a wave–particle resonance in the parallel direction, which means that it may not be recovered in the fluid model perfectly. This fact motivates us to utilize a gyrokinetic (GK) model as will be described in Sec. IV.

IV. GYROKINETIC DESCRIPTION
A. Dispersion relation

For a gyrokinetic description of source-driven SSU and GAM, we consider a GK equation for the zonal component, which is given by

$$\left(\frac{\partial}{\partial t} + v_\parallel \hat{\mathbf{b}} \cdot \nabla + i \omega_D \right) \delta f_{\mathbf{k}_\perp}^{(g)}$$
$$= -\left(v_\parallel \hat{\mathbf{b}} \cdot \nabla + i \omega_D \right) \left(F_0 J_0 \frac{e \phi_{\mathbf{k}_\perp}}{T} \right) - \mathbf{v}_E \cdot \nabla F_0. \tag{22}$$

Equation (22) is different from Eq. (13) in twofold. First, the $\mathbf{E} \times \mathbf{B}$ convective term is applied to the equilibrium distribution function F_0

instead of the perturbed one $f_{\mathbf{k}_\perp}^{(g)}$. Second, the poloidal source term $S_{\mathbf{k}_\perp}F_0$ is removed. It is because finding a kinetic equilibrium of Eq. (13), that is, exactly equivalent to the fluid model, is unattainable. Instead, we assume that F_0 is not simple local Maxwellian but has a poloidally inhomogeneous equilibrium flow $\tilde{u}_{\parallel\mathbf{k}_\perp}^{Eq}$ to offset the density source $\tilde{S}_{\mathbf{k}_\perp}^{\delta n}F_M$. Then, the newly defined local equilibrium distribution function is given in the form of

$$F_0 = \frac{n_0}{(2\pi T/m)^{3/2}}\exp\left[-\frac{\left(v_\parallel - \tilde{u}_{\parallel\mathbf{k}_\perp}^{Eq}\right)^2 + v_\perp^2}{2T/m}\right]$$
$$\simeq F_M\left(1 + \frac{v_\parallel \tilde{u}_{\parallel\mathbf{k}_\perp}^{Eq}}{v_T^2}\right) = F_M\left(1 + \frac{v_\parallel}{v_T}\int d\theta\,\frac{\tilde{S}_{\mathbf{k}_\perp}^{\delta n}}{n_0\omega_{ti}}\right), \quad (23)$$

where the normalized poloidal source $\hat{S} \equiv \tilde{S}_{\mathbf{k}_\perp}^{\delta n}/(n_0\omega_{ti})$ and the corresponding equilibrium flow $\hat{u}_{\parallel\mathbf{k}_\perp} \equiv \tilde{u}_{\parallel\mathbf{k}_\perp}^{Eq}/v_{Ti}$ are assumed to be order $\mathcal{O}(\varepsilon)$ and terms with higher orders are neglected. For the perpendicular wave number adopted in $\tilde{S}_{\mathbf{k}_\perp}^{\delta n}$ and $\tilde{u}_{\parallel\mathbf{k}_\perp}^{Eq}$, we use the same condition assumed in Sec. III. Thus, the last term on the right hand side of Eq. (22) operated as a driver for source-driven modes, rather than a turbulence driver. This new F_0 satisfies the fluid equilibrium conditions of both the rMHD and GLF4M models shown in Eqs. (11) and (20a), respectively. Hereafter, we only consider an in–out asymmetric particle source because the up–down asymmetric one does not drive source-driven modes as demonstrated in Secs. II and III.

In deriving a GK dispersion relation, we follow Ref. 22, which originally considers the collisionless damping of GAM. Considering passing ions, we neglect the mirror term and rewrite Eq. (22) as

$$\left(\frac{\partial}{\partial t} + \frac{v_\parallel}{qR_0}\frac{\partial}{\partial\theta}\right)\left(e^{ik_r\hat{\delta}\cos\theta}\delta\hat{f}_{\mathbf{k}_\perp}\right)$$
$$= -\frac{v_\parallel}{qR_0}\frac{\partial}{\partial\theta}\left(e^{ik_r\hat{\delta}\cos\theta}J_0\frac{e\phi_{\mathbf{k}_\perp}}{T}\right) - \left(e^{ik_r\hat{\delta}\cos\theta}\mathbf{v}_E\cdot\nabla\hat{F}_0\right), \quad (24)$$

where $\delta\hat{f}_{\mathbf{k}_\perp} \equiv \delta f_{\mathbf{k}_\perp}/F_M$, $\hat{F}_0 \equiv F_0/F_M$, $\hat{\delta} \equiv (\varepsilon/\Omega_p)[v_\parallel + \mu B_0/(mv_\parallel)]$, and $\Omega_p = eB_p/(mc)$. Here, $\hat{\delta}\cos\theta$ represents the radial displacement of the passing ion. Using Fourier–Laplace transform, a perturbed distribution function including a poloidally inhomogeneous source can be calculated from Eq. (24) giving rise to

$$\delta\hat{f}_{k_r,m}(\omega) = \sum_{l,l'}i^{l'-l}J_l(k_r\hat{\delta})J_{l'}(k_r\hat{\delta})\left(\frac{(m+l)(v_\parallel/qR_0)}{\omega - (m+l)(v_\parallel/qR_0)}\right)$$
$$\times\left(\frac{e\hat{\phi}_{k_r,m+l-l'}(\omega)}{T} + \frac{q}{\varepsilon}\left(\frac{k_r a_i}{2}\right)\frac{\tilde{S}_{k_r,c}^{\delta n}}{n_0\omega_{ti}}\left(\frac{e\hat{\phi}_{k_r,0}(\omega)}{T}\right)\right)$$
$$\times\left\{\sum_{l,l''}i^{l''-l}J_l(k_r\hat{\delta})J_{l''}(k_r\hat{\delta})\left(\delta_{l-l''}^{m+1} + \delta_{l-l''}^{m-1}\right)\right.$$
$$\left.\times\left(\frac{(v_\parallel/qR_0)}{\omega - (m+l)(v_\parallel/qR_0)}\right)\right\} + \delta\hat{I}_{k_r,m}(\omega), \quad (25)$$

where $\delta\hat{I}_{k_r,m}(\omega)$ denotes the initial condition term and δ_j^i is the Kronecker delta. In deriving Eq. (25), the small gyroradius limit $k_\perp\rho \to 0$ has been used. The second term proportional to $\tilde{S}_{k_r,c}^{\delta n}$ in Eq. (25) represents the poloidal source effect. From Eq. (25), one can derive $\delta\hat{f}_{k_r,\pm1}$ as

$$\delta\hat{f}_{k_r\pm1}(\omega) = \frac{\pm(v_\parallel/qR_0)}{\omega \mp (v_\parallel/qR_0)}\left[\frac{e\phi_{k_r\pm1}(\omega)}{T}\right.$$
$$\left. + i\left\{\left(\frac{k_r\hat{\delta}}{2}\right) \mp i\frac{\hat{S}_c}{\varepsilon}\left(\frac{k_r a_i q}{2}\right)\right\}\frac{e\phi_{k,0}(\omega)}{T}\right], \quad (26)$$

where $\hat{S}_c \equiv \tilde{S}_{k_r,c}^{\delta n}/(n_0\omega_{ti})$ and the terms $\phi_{k_r,m}$ with $|m| \geq 2$ are neglected owing to their smallness. We also neglect the higher harmonic resonance occurring at $\omega = n\,v_\parallel/(qR_0)$ $(n = 2, 3, 4\ldots)$, which actually enhance Landau damping by the finite-orbit-width (FOW) of passing ions.[25] By substituting $\delta\hat{f}_{k_r\pm1}$ given above into Eqs. (2.4) and (2.5) of Ref. 25, which are omitted for simplicity, we finally obtain the GK dispersion relation with the poloidal source effect

$$K_{GK}^{-1}(\hat{\omega}) = -i\frac{\hat{\omega}}{\sqrt{2}} - i\frac{q^2}{2}\left[\left\{2Z_4\left(\frac{\hat{\omega}}{\sqrt{2}}\right) + 2Z_2\left(\frac{\hat{\omega}}{\sqrt{2}}\right) + Z_0\left(\frac{\hat{\omega}}{\sqrt{2}}\right)\right\}\right.$$
$$- \frac{\hat{\omega}}{2\sqrt{2}}\frac{\left\{2Z_2\left(\frac{\hat{\omega}}{\sqrt{2}}\right) + Z_0\left(\frac{\hat{\omega}}{\sqrt{2}}\right)\right\}^2}{\tau_i + Z_1\left(\frac{\hat{\omega}}{\sqrt{2}}\right)}$$
$$- \left\{2Z_3\left(\frac{\hat{\omega}}{\sqrt{2}}\right) + Z_1\left(\frac{\hat{\omega}}{\sqrt{2}}\right)\right\}\frac{i\hat{S}_c}{\sqrt{2}\varepsilon}$$
$$\left. + \frac{\hat{\omega}}{\sqrt{2}}\frac{Z_1\left(\frac{\hat{\omega}}{\sqrt{2}}\right)\left\{2Z_2\left(\frac{\hat{\omega}}{\sqrt{2}}\right) + Z_0\left(\frac{\hat{\omega}}{\sqrt{2}}\right)\right\}}{\tau_i + Z_1\left(\frac{\hat{\omega}}{\sqrt{2}}\right)}\frac{i\hat{S}_c}{\sqrt{2}\varepsilon}\right], \quad (27)$$

when it satisfies $\phi_{k,0}(\hat{\omega}) = K(\hat{\omega})\cdot\phi_{k,0}(t = 0)$. Here, Z_n is the newly defined plasma dispersion function whose expression is given in Appendix D. In Eq. (27), the first two terms in the bracket on the right hand side represent Landau damping due to resonance at $v_\parallel = qR_0$, while the remaining terms, which is proportional to $\hat{S}_c/\varepsilon$, denote the poloidal source effect. One can easily find that, if there is no poloidal source $\hat{S}_c = 0$, Eq. (27) is reduced to results given by Sugama and Watanabe[22] and Gao et al.[23] when neglecting the resonance term at $\omega = 2v_\parallel/qR_0$ and also the result given by Zonca and Chen,[16] which shows the degeneracy between GAM and beta-induced Alfvén eigenmodes in the limit of $\omega_*/\omega \to 0$.

B. Source threshold: Comparison between GK and GLF4M models

By numerically solving the dispersion relations, Eqs. (27) for the GK model and (21) for the GLF4M model, we can compute and compare the real frequency and the growth rate of SSU and GAM. In addition, we conduct parameter scans of threshold source intensity for SSU and GAM with respect to ε, q, and τ_e. Because either SSU or GAM is destabilized depending on the deposited location of the particle source, we investigate them as a function of outboard and inboard source intensity, separately.

In Fig. 3, the frequency (ω^{SSU}) and the growth rate (γ^{SSU}) of SSU are plotted as a function of the outboard source intensity ($\hat{S}_{out} = \hat{S}_c > 0$) for fixed parameters ($\varepsilon$, q, τ_e) = (0.1, 1.4, 1.13). Here, dotted and solid curves represent ω^{SSU} and γ^{SSU}, respectively, while the red
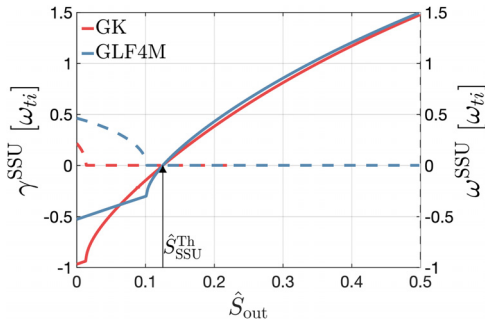
FIG. 3. Real frequency (ω^{SSU}, dotted) and growth rate (γ^{SSU}, solid) of SSU as a function of the outboard source intensity ($\hat{S}_{\mathrm{out}}$). Results are obtained by numerically solving GK [Eq. (27), red] and GLF4M [Eq. (21), blue] dispersion relations when $(\varepsilon, q, \tau_e) = (0.1, 1.4, 1.13)$.

FIG. 4. Threshold source intensity for SSU ($\hat{S}_{\mathrm{SSU}}^{\mathrm{Th}}$) as a function of the (a) inverse aspect ratio ε, (b) safety factor q, and (c) electron to ion temperature ratio τ_e. Results are obtained using the GK [Eq. (27), red circles] and the GLF4M [Eq. (21), blue diamonds] dispersion relations. Analytical expression for $\hat{S}_{\mathrm{SSU}}^{\mathrm{Th}}$ given in Eq. (28) is also plotted by black dotted lines. All parameters are fixed as $(\varepsilon, q, \tau_e) = (0.1, 1.4, 1.13)$ except for the one being used as a variable.

and blue curves depict the result from GK and GLF4M models, respectively. As shown in Fig. 3, deviation between two models is obvious when the source intensity is lower than the source threshold. However, when the source intensity is higher than the threshold, the deviation diminishes significantly. Also, γ^{SSU} from each model shows a good agreement. One more interesting fact here is that ω^{SSU} and γ^{SSU} from GK and GLF4M formulations coincide well when $(\omega, \gamma) \to 0$ as plotted by a black arrow around $\hat{S}_{\mathrm{out}} \simeq 0.12$ in Fig. 3. It means that the source threshold predicted by each model has a same value. To verify this, we derive an expression for a source threshold of SSU ($\hat{S}_{\mathrm{SSU}}^{\mathrm{Th}}$) by taking Taylor expansion around $\omega = 0$ in Eqs. (27) and (21), respectively, which is given in the form of

$$\hat{S}_{\mathrm{SSU|GLF4M}}^{\mathrm{Th}} = \frac{\varepsilon}{\chi} = \varepsilon\sqrt{\frac{\pi}{2}} = \hat{S}_{\mathrm{SSU|GK}}^{\mathrm{Th}}. \tag{28}$$

Here, $\hat{S}_{\mathrm{SSU|GLF4M}}^{\mathrm{Th}}$ and $\hat{S}_{\mathrm{SSU|GK}}^{\mathrm{Th}}$ denote the source threshold derived from the GLF4M and the GK models, respectively. One can find that both models yield the same value. This is because the closure coefficient χ is determined by matching fluid response to the kinetic one in the low frequency limit ($\omega \to 0$). Therefore, results of both GLF4M and GK models perfectly match for SSU due to its zero-frequency ($\omega^{\mathrm{SSU}} = 0$) nature.

Next, parameter scans of $\hat{S}_{\mathrm{SSU}}^{\mathrm{Th}}$ using GK (red circles) and GLF4M (blue diamonds) dispersion relations are conducted with respect to ε, q, and τ_e whose results are plotted in Figs. 4(a), 4(b), and 4(c), respectively. The analytic result in Eq. (28) is also presented by black dotted lines. In each figure, the same parameters to produce Fig. 3 are used except for the one being utilized as a variable. One can see that results from GK and GLF4M models coincide in overall parameter ranges. Also, the analytical results are perfectly matched with the numerical ones. Again, it is due to the fact that the closure coefficient χ is approximated in the low-frequency limit ($\omega \to 0$). For the case of GAM ($\omega \sim v_{T_i}/R_0$), however, some deviations are inevitable as will be shown shortly.

Figure 5 shows the frequency (ω^{GAM}) and the growth rate (γ^{GAM}) of GAM as a function of the inboard source intensity ($\hat{S}_{\mathrm{in}} = -\hat{S}_c > 0$) using the same parameters in Fig. 3. The results from GK and GLF4M dispersion relations are plotted with the same colors used in Fig. 3. As mentioned earlier, the discrepancy between the two
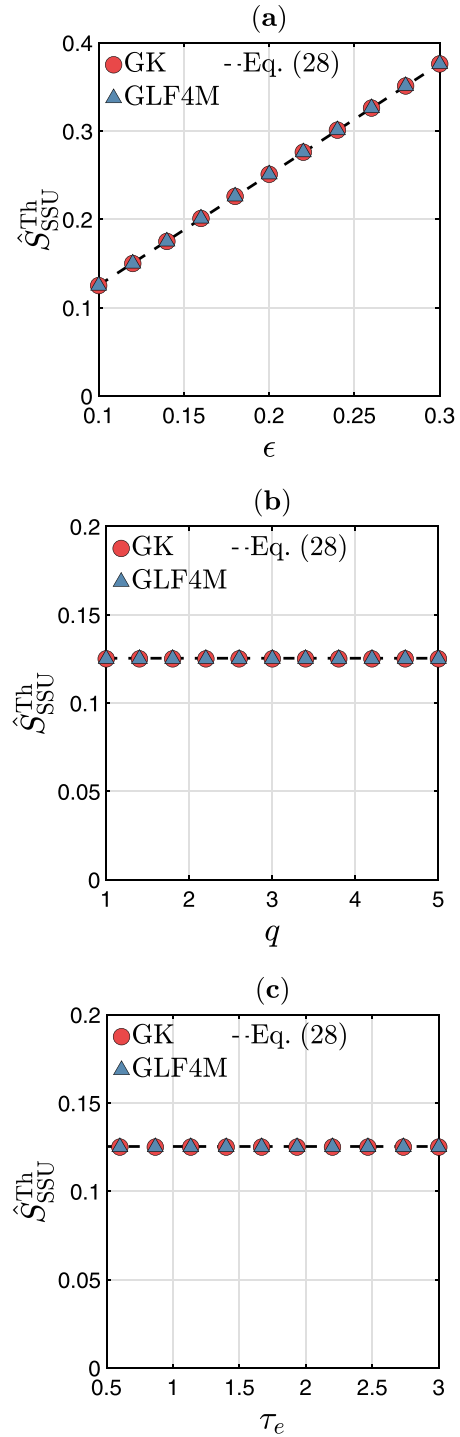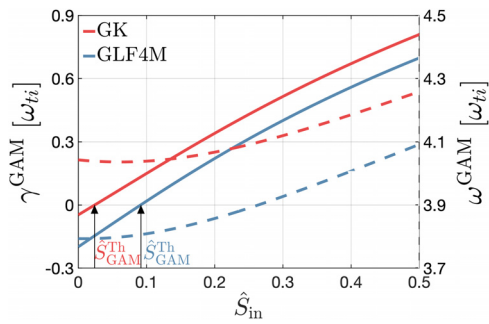
FIG. 5. Real frequency (ω^{GAM}, dotted) and growth rate (γ^{GAM}, solid) of GAM as a function of the inboard source intensity ($\hat{S}_{\text{in}}$). Results are obtained by numerically solving the GK [Eq. (27), red] and the GLF4M [Eq. (21), blue] dispersion relations when $(\varepsilon, q, \tau_e) = (0.1, 1.4, 1.13)$.

models is inevitable for the case of GAM because the effect of Landau damping is approximated in the GLF4M model with a fifth-order polynomial, while it is fully captured in the GK model through plasma dispersion functions. As shown in Fig. 5, although both models show a similar tendency, GLF4M somewhat underestimate both ω^{GAM} and γ^{GAM}. This implies that the Hammet–Perkins closure model gives a stronger damping of the wave and subsequently the source threshold for GAM ($\hat{S}_{\text{GAM}}^{\text{Th}}$) can be overestimated as indicated by black arrows in Fig. 5.

Results of parameter scans for $\hat{S}_{\text{GAM}}^{\text{Th}}$ in terms of ε, q, and τ_e are shown in Figs. 6(a), 6(b), and 6(c), respectively. In Fig. 6, same colors and symbols in Fig. 4 are used to represent results obtained from GK and GLF4M dispersion relations. Also, the same parameters used in Fig. 4 are used except for the one being used as a variable. In contrast to the SSU case shown in Fig. 4, two models show some discrepancy. Specifically, we find that $\hat{S}_{\text{GAM}}^{\text{Th}}$ for each model exhibits distinct functional dependence on q^2 and τ_e. In the GK model, Landau damping induces exponential damping to the threshold [i.e., $\hat{S}_{\text{GAM}|\text{GK}}^{\text{Th}} \propto \varepsilon \exp(-q^2) \exp(-\tau_e)$]. On the other hand, in the GLF4M model, the analytic expression for $\hat{S}_{\text{GAM}}^{\text{Th}}$ is derived as

$$
\hat{S}_{\text{GAM}|\text{GLF4M}}^{\text{Th}} = \varepsilon\chi \left[\frac{5}{2(2 + \tau_e)} + \frac{1}{q^2} \right.
$$
$$
\left. \times \frac{(7 + 4\tau_e)\{26 - 24\chi^2 + 27(1 - \chi^2)\tau_e + 7\tau_e^2\}}{(14 + 15\tau_e + 4\tau_e^2)^2} \right]
$$
$$(29)$$

using the GLF4M dispersion relation. Here, the small terms of order $\mathcal{O}(q^{-n})$ with $n \geq 4$ are neglected. The analytic result presented in Eq. (29) is also plotted by blue dotted curves in Fig. 6. As shown in Fig. 6, Landau damping causes an exponential damping of $\hat{S}_{\text{GAM}}^{\text{Th}}$ with regard to q^2 and τ_e in the GK model, while it does an algebraic damping in the GLF4M model. The GLF4M model even predict a finite value of the source threshold $\hat{S}_{\text{GAM}|\text{GLF4M}}^{\text{Th}} = \frac{5}{2}\varepsilon\chi/(2 + \tau_e)$ in high q limit. This discrepancy between models is because Landau damping, which brings about a significant damping to GAM can be fully reproduced only with the GK model, while the GLF4M one captures it approximately. Thus, for an accurate evaluation of the source threshold, the GLF4M model is sufficient for SSU, while a GK model is inevitable for GAM.
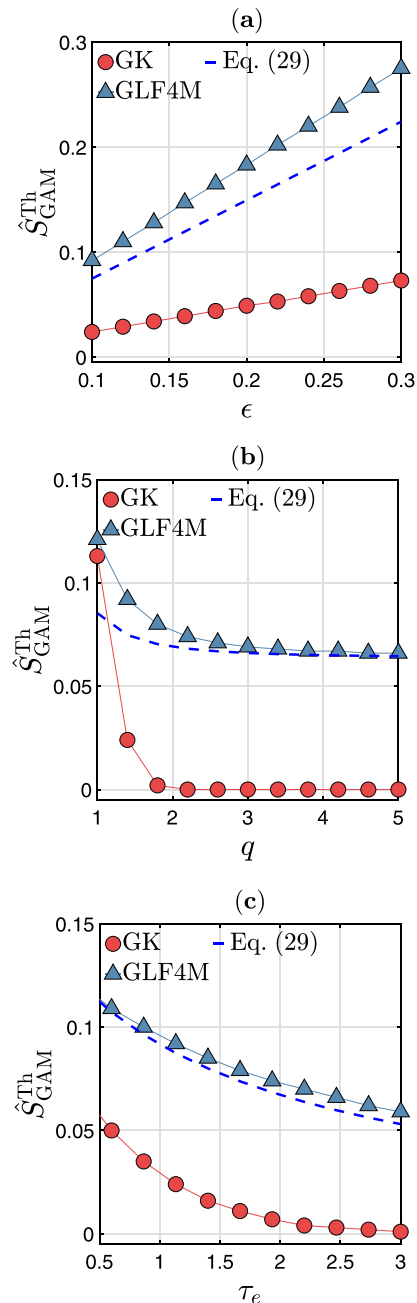

FIG. 6. Threshold source intensity for GAM ($\hat{S}_{\text{GAM}}^{\text{Th}}$) as a function of (a) inverse aspect ratio ε, (b) safety factor q, and (c) electron to ion temperature ratio τ_e. Results are obtained using the GK [Eq. (27), red circles] and the GLF4M [Eq. (21), blue diamonds] dispersion relations. All parameters are fixed as $(\varepsilon, q, \tau_e) = (0.1, 1.4, 1.13)$ except for the one being used as a variable.

V. SUMMARY AND CONCLUSIONS

The poloidal $\mathbf{E} \times \mathbf{B}$ flow has a profound influence on turbulent transport and confinement of tokamak plasmas. In this paper, we have studied the impact of the poloidally asymmetric particle source on the

generation of axisymmetric poloidal $\mathbf{E} \times \mathbf{B}$ flow. We first review the work by Hassam and Drake[8] who finds out that a poloidal source can destabilize either SSU or GAM depending on its deposition location. To capture the effect of Landau damping, we employ a GLF4M model in place of rMHD one by Hassam and adopt the Hammet–Perkins closure. With the GLF4M model, the poloidal $\mathbf{E} \times \mathbf{B}$ flow is generated by the destabilization of either SSU or GAM. The SSU and GAM are driven by outboard and inboard sources, respectively. This result is consistent with that in the rMHD model. In fact, we have shown that the dispersion relation obtained from the GLF4M model yields the same one that derived from the rMHD model under an appropriate condition in Appendix C.

The crucial difference between the two models is that the GLF4M model predicts the presence of the source threshold. It is well known that GAM is usually Landau damped out due to its fast frequency ($\omega_{GAM} \sim v_{T_i}/R_0$) comparable to the transit one [$\omega_{ti} \sim v_{T_i}/(qR_0)$ $\sim \omega_{GAM}/q$]. Thus, it is quite obvious for the GLF4M model to predict the source threshold for GAM. However, one interesting point not emphasized in this paper is that Landau damping affects not only GAM but also SSU, which is found to have zero-frequency from the rMHD model. Note that there is no parallel resonance for SSU due to its zero frequency. However, in fact, SSU is found to have a finite frequency when the source is not intense enough with both GLF4M and GK results as one can see that ω^{SSU} has finite value when $\hat{S}_{out} \lesssim \hat{S}_{SSU}^{Th}$ in Fig. 3. Thus, the threshold for SSU can be affected by the Landau damping.

To substantiate that Landau damping does have an influence on these source driven instabilities, we make a further analysis using a GK model that captures the full effect of Landau damping. Then, using dispersion relations derived from GLF4M and GK models, we calculate the frequency and the growth rate of each mode in terms of source intensity. This procedure allows us to conduct parameter scans of source threshold with regard to ε, q, and τ_e. For the case of SSU driven by an outboard source, the growth rates calculated from both models are consistent once the source intensity is higher than the threshold ($\hat{S}_{out} > \hat{S}_{SSU}^{Th}$) as shown in Fig. 3. We also have shown that $\hat{S}_{SSU}^{Th}$ for both models is identical as presented in Eq. (28). The reason for this identity is because the closure coefficient χ is evaluated in the low-frequency limit ($\omega \to 0$). On the other hand, for the case of GAM driven by an inboard source, the real frequency and the growth rate calculated from each model deviate in overall range of the inboard source intensity as shown in Fig. 5. The parametric dependence of $\hat{S}_{GAM}^{Th}$ on ε, q, and τ_e also differs by model as shown in Fig. 6. It is because the GLF4M model overestimates the Landau damping effect. specifically, the GLF4M model that considers only a few finite-order fluid variables is unable to reproduce the exponential damping of $\hat{S}_{GAM}^{Th}$ with regard to q^2 and τ_e given by the GK dispersion.

On the basis of these results, one can conclude that Landau damping may determine the critical particle source throughput beyond which an instability sets in. At this point, it is instructive to estimate $\hat{S}_c$ from a model of low field side (LFS) pellet fueling system in a tokamak. We consider the ITER pellet injector that has been designed with the maximum throughput of $120\,\text{Pa}\,\text{m}^3\,\text{s}^{-1}$ and $v_p = 300\,\text{m}\,\text{s}^{-1}$ (v_p: pellet speed). Suppose a pellet injector with the throughput $R\,\text{Pa}\,\text{m}^3\,\text{s}^{-1}$ and the pellet speed v_p. Then, the number of particles deposited to the tokamak per unit time is

$$N = \frac{2R}{m_p v_p^2},\qquad(30)$$

where m_p is the fuel ion mass. If we assume that injected particles occupy volume V' with maximal poloidal asymmetry, then the normalized number of particles deposited during a transit time is

$$\hat{N} = \frac{4\pi R}{m_p v_p^2 V' n_0 \omega_{ti}}.\qquad(31)$$

One can easily recognize that Eq. (31) relates the amount of particles injected by a realistic pellet injection system[30] $\hat{N}$ to the outboard source intensity $\hat{S}_{out}$ in this paper. As an example, if we assume that the pellet deposition radius is given by $0.8 < r/a < 1.0$,[30] one can obtain the range of $\hat{S}_{out}$, which is given as $0.02 \lesssim \hat{S}_{out} \lesssim 0.1$, from Eq. (31). Here, $\hat{S}_{out}$ is given as a range because it depends on n_0, T_i, and q whose values are determined by the deposited position of the pellet. For the ITER case, $0.1 < n_0 < 1.0\,[10^{20}\,\text{atoms}\,\text{m}^{-3}]$, $4 < T_i < 10\,(\text{keV})$, and $1.6 < q < 3.5$ are used to calculate $\hat{S}_{out}$. The maximum value of $\hat{S}_{out}(\sim 0.1)$ is smaller or quite close to $\hat{S}_{SSU}^{Th}$ in Fig. 4. Therefore, one can expect that the LFS pellet system in ITER may excite SSU if maximum throughput is applied. Here, we take a pellet injection system as an illustrative example inducing a poloidally asymmetric density. It realistic tokamak experiments, sources of poloidal asymmetry will arise, but not limited to, from inhomogeneous turbulent transport and/or the mechanical structure. It will be of interest if the theory presented in this paper is verified with more experiments and simulations.

AUTHOR DECLARATIONS
Conflict of Interest

The authors have no conflicts to disclose.

Author Contributions

YoungHoon Lee: Investigation (lead); Software (lead); Writing – original draft (lead). **Hogun Jhang:** Validation (lead); Writing – review & editing (equal). **Sung Sik Kim:** Formal analysis (lead); Writing – review & editing (equal). **Jungpyo Lee:** Conceptualization (lead); Project administration (lead); Writing – original draft (supporting); Writing – review & editing (equal).

DATA AVAILABILITY

The data that support the findings of this study are available from the corresponding author upon reasonable request.

APPENDIX A: DEFINITIONS AND THE GYRO-AVERAGING OPERATORS FOR GLF4M MODEL

In this appendix, all the missing definitions and messy coefficients used in Sec. II are given. Fluid variables up to the second order, which are used for time evolution, are defined as

$$[\delta n_{\mathbf{k}_\perp}, n_0 u_{\|\mathbf{k}_\perp}, \delta p_{\|\mathbf{k}_\perp}, \delta p_{\perp\mathbf{k}_\perp}] = \int d^3v \, \delta f_{\mathbf{k}_\perp}^{(g)}\left[1, v_\|, mv_\|^2, \frac{1}{2}mv_\perp^2\right],$$
(A1)

where quantities inside the bracket in the left hand side represent gyrocenter density, parallel velocity, parallel, and perpendicular pressures. In the same manner, the source terms corresponding to them are defined as

$$\left[S_{\mathbf{k}_\perp}^{\delta n}, S_{\mathbf{k}_\perp}^{u_\|}, S_{\mathbf{k}_\perp}^{\delta p_\|}, S_{\mathbf{k}_\perp}^{\delta p_\perp}\right] = \int d^3v \, S_{\mathbf{k}_\perp} F_0\left[1, mv_\|, mv_\|^2, \frac{1}{2}mv_\perp^2\right].$$
(A2)

The third- (parallel heat fluxes) and fourth-order fluid variables are defined as

$$[q_{\|\mathbf{k}_\perp}, q_{\perp\mathbf{k}_\perp}] = \int d^3v \, \delta f_{\mathbf{k}_\perp}^{(g)} v_\|\left[\left(mv_\|^2 - 3T\right), \left(\frac{1}{2}mv_\perp^2 - T\right)\right],$$
(A3)

$$[\delta r_{\|,\|\mathbf{k}_\perp}, \delta r_{\|,\perp\mathbf{k}_\perp}, \delta r_{\perp,\perp\mathbf{k}_\perp}] = \int d^3v \, \delta f_{\mathbf{k}_\perp}^{(g)} m\left[v_\|^4, \frac{1}{2}v_\|^2 v_\perp^2, \frac{1}{4}v_\perp^4\right].$$
(A4)

These higher order variables must be expressed in terms of lower order fluid variables by taking an appropriate closure model. In our GLF4M model, the Landau and Maxwellian closures are employed for them, respectively. Also, note that perturbed parallel and perpendicular temperatures $(\delta T_{\|\mathbf{k}_\perp}, \delta T_{\perp\mathbf{k}_\perp})$ are determined by the following relations:

$$\delta p_{\|\mathbf{k}_\perp} = n_0 \delta T_{\|\mathbf{k}_\perp} + T \delta n_{\mathbf{k}_\perp},$$
$$\delta p_{\perp\mathbf{k}_\perp} = n_0 \delta T_{\perp\mathbf{k}_\perp} + T \delta n_{\mathbf{k}_\perp}.$$
(A5)

For appropriate gyro-averaging operators, we use simple approximations given elsewhere.[29] As simply mentioned in Sec. III, the velocity space average of J_0 is approximated as $\langle J_0\rangle \simeq e^{-b/2}$. One can easily find that $\Gamma_0^{1/2}$ is replaced by $e^{-b/2}$ for $\langle J_0\rangle$ in Eq. (20) of Ref. 29. Because we consider the long-wavelength scale with $k_\perp\rho \sim \mathcal{O}(\varepsilon)$ in this study, approximating $\langle J_0\rangle$ to $e^{-b/2}$ instead of $\Gamma_0^{1/2}$, which are devised to compensate a discrepancy between Γ_0 and $e^{-b/2}$ when deriving linear dispersion relation for large b,[27] causes no technical difficulty. Other gyro-averaging operators, which recover the finite Larmor radius (FLR) effect, are given by

$$\frac{1}{2}\hat{\nabla}_\perp^2\left(\langle J_0\rangle\phi_{\mathbf{k}_\perp}\right) = b\frac{\partial\langle J_0\rangle}{\partial b}\phi_{\mathbf{k}_\perp},$$
$$\hat{\hat{\nabla}}_\perp^2\left(\langle J_0\rangle\phi_{\mathbf{k}_\perp}\right) = b\frac{\partial^2}{\partial b^2}\left(b\langle J_0\rangle\right)\phi_{\mathbf{k}_\perp},$$
(A6)

which correspond to Eqs. (26) and (27) of Ref. 29, respectively.

APPENDIX B: DERIVATION OF THE DISPERSION RELATION FROM GLF4M EQUATIONS

In this appendix, we derive a linear dispersion relation from the GLF4M model presented in Eq. (21). Here, we follow the same procedure used in Appendixes B–D of Ref. 25, which derive a GAM dispersion relation from gyrofluid equations. To start, we subtract equilibrium conditions shown in Eqs. (19a)–(19c) from GLF4M Eqs. (15a)–(15d) to separate equilibrium part and the perturbed one. Then, equations for the perturbed part are given in the form of

$$\frac{\partial\delta n_{\mathbf{k}_\perp}}{\partial t} + \mathbf{B}\cdot\nabla\frac{n_0 u_{\|\mathbf{k}_\perp}}{B} + i\omega_D\left(\frac{\delta p_{\|\mathbf{k}_\perp} + \delta p_{\perp\mathbf{k}_\perp}}{T}\right)$$
$$= -\left(2 + \frac{1}{2}\hat{\nabla}_\perp^2\right)i\omega_D\frac{e\phi_{\mathbf{k}_\perp}}{T}e^{-b/2},$$
(B1)

$$mn_0\frac{\partial u_{\|\mathbf{k}_\perp}}{\partial t} + \mathbf{u}_E\cdot\nabla\tilde{u}_{\|\mathbf{k}_\perp}^{Eq} + \mathbf{B}\cdot\nabla\frac{\delta p_{\|\mathbf{k}_\perp}}{B}$$
$$+ \delta p_{\perp\mathbf{k}_\perp}\nabla_\|\ln B + i\omega_D\left(\frac{q_{\|\mathbf{k}_\perp} + q_{\perp\mathbf{k}_\perp} + 4p_0 u_{\|\mathbf{k}_\perp}}{T/m}\right)$$
$$= -n_0 e\left(\mathbf{B}\cdot\nabla\frac{\phi_{\mathbf{k}_\perp}}{B}e^{-b/2} + \frac{1}{2}\hat{\nabla}_\perp^2\phi_{\mathbf{k}_\perp}e^{-b/2}\nabla_\|\ln B\right),$$
(B2)

$$\frac{\partial\delta p_{\|\mathbf{k}_\perp}}{\partial t} + \mathbf{B}\cdot\nabla\left(\frac{q_{\|\mathbf{k}_\perp} + 3p_0 u_{\|\mathbf{k}_\perp}}{B}\right) + 2\left(q_{\|\mathbf{k}_\perp} + 3p_0 u_{\|\mathbf{k}_\perp}\right)\nabla_\|\ln B$$
$$+ i\omega_D\left(\frac{\delta r_{\|,\|\mathbf{k}_\perp} + \delta r_{\|,\perp\mathbf{k}_\perp}}{T/m}\right) = -\left(4 + \frac{1}{2}\hat{\nabla}_\perp^2\right)i\omega_D p_0\frac{e\phi_{\mathbf{k}_\perp}}{T}e^{-b/2},$$
(B3)

$$\frac{\partial\delta p_{\perp\mathbf{k}_\perp}}{\partial t} + \mathbf{B}\cdot\nabla\left(\frac{q_{\perp\mathbf{k}_\perp} + p_0 u_{\|\mathbf{k}_\perp}}{B}\right) - \left(q_{\perp\mathbf{k}_\perp} + p_0 u_{\|\mathbf{k}_\perp}\right)\nabla_\|\ln B$$
$$+ i\omega_D\left(\frac{\delta r_{\|,\perp\mathbf{k}_\perp} + \delta r_{\perp,\perp\mathbf{k}_\perp}}{T/m}\right)$$
$$= -\left(3 + \frac{3}{2}\hat{\nabla}_\perp^2 + \hat{\hat{\nabla}}_\perp^2\right)i\omega_D p_0\frac{e\phi_{\mathbf{k}_\perp}}{T}e^{-b/2}.$$
(B4)

Hereafter, we use the following normalization:

$$\left[t\frac{v_T}{qR_0}, \frac{\delta n_{\mathbf{k}_\perp}}{n_0}, \frac{u_{\|\mathbf{k}_\perp}}{v_T}, \frac{u_{E\mathbf{k}_\perp}}{v_T}, \frac{\delta p_{\|\mathbf{k}_\perp}}{p_0}, \frac{\delta p_{\perp\mathbf{k}_\perp}}{p_0}, \frac{\tilde{u}_{\|\mathbf{k}_\perp}^{Eq}}{v_T}, \frac{\tilde{S}_{\mathbf{k}_\perp}^{\delta n}}{n_0\omega_{ti}}\right]$$
$$\rightarrow \left[t, \delta n, u_\|, u_E, \delta p_\|, \delta p_\perp, u_\|^{Eq}, S\right],$$
$$\left[\frac{e\phi_{\mathbf{k}_\perp}}{T}, \frac{q_{\|\mathbf{k}_\perp}}{p_0 v_T}, \frac{q_{\perp\mathbf{k}_\perp}}{p_0 v_T}, \frac{\delta r_{\|,\|\mathbf{k}_\perp}}{p_i v_T^2}, \frac{\delta r_{\|,\perp\mathbf{k}_\perp}}{p_i v_T^2}, \frac{\delta r_{\perp,\perp\mathbf{k}_\perp}}{p_i v_T^2}\right]$$
$$\rightarrow \left[\hat{\phi}, \hat{q}_\|, \hat{q}_\perp, \delta\hat{r}_{\|,\|}, \delta\hat{r}_{\|,\perp}, \delta\hat{r}_{\perp,\perp}\right].$$
(B5)

Then, using the normalization (B5), the perturbed Eqs. (B1)–(B4) can be rewritten as

$$\frac{\partial\delta\hat{n}}{\partial t} + \frac{\partial\hat{u}_\|}{\partial\theta} - \varepsilon\hat{u}_\|\sin\theta = i(k_r\rho_{ti}q)\sin\theta\left[\delta\hat{p}_\| + \delta\hat{p}_\perp + 2\hat{\phi}\right],$$
(B6)

$$\frac{\partial\hat{u}_\|}{\partial t} + \frac{q}{\varepsilon}\hat{u}_E\frac{\partial\tilde{u}_\|^{Eq}}{\partial\theta} + \frac{\partial\delta\hat{p}_\|}{\partial\theta} + \varepsilon\sin\theta\left(\delta\hat{p}_\perp - \delta\hat{p}_\|\right)$$
$$= i(k_r\rho_{ti}q)\sin\theta\left(\hat{q}_\| + \hat{q}_\perp + 4\hat{u}_\|\right) - \frac{\partial\hat{\phi}}{\partial\theta},$$
(B7)

$$\frac{\partial\delta\hat{p}_\|}{\partial t} + \frac{\partial\left(\hat{q}_\| + 3\hat{u}_\|\right)}{\partial\theta} + \varepsilon\sin\theta\left(2\hat{q}_\perp - \hat{q}_\| - \hat{u}_\|\right)$$
$$= i(k_r\rho_{ti}q)\sin\theta\left[\delta\hat{r}_{\|\||} + \delta\hat{r}_{\|\perp} + 4\hat{\phi}\right],$$
(B8)

$$\frac{\partial\delta\hat{p}_\perp}{\partial t} + \frac{\partial\left(\hat{q}_\perp + \hat{u}_\|\right)}{\partial\theta} - 2\varepsilon\sin\theta\left(\hat{q}_\perp + \hat{u}_\|\right)$$
$$= i(k_r\rho_{ti}q)\sin\theta\left[\delta\hat{r}_{\|\perp} + \delta\hat{r}_{\perp\perp} + 3\hat{\phi}\right].$$
(B9)

Here, we assume a long wavelength perturbation ($k_r \rho_{ti} < 1$) and the large aspect-ratio tokamak ($\varepsilon \ll 1$) with concentric circular surfaces. The small terms of the order $\mathcal{O}(\varepsilon^2) \sim \mathcal{O}(b_i)$ are neglected, where $b_i = (k_r \rho_{ti})^2$. Now, each equation can be divided into three components of 0, c, and s, each of which corresponds to the Fourier coefficient of $m = 0$, $\sin\theta$, and $\cos\theta$ component, respectively. However, we do not represent all the components here but only the components those contribute to the dispersion relation (i.e., $\delta\hat{n}_s$, $\hat{u}_{\|c}$, $\delta\hat{n}_0$, $\hat{p}_{\|s}$, and $\hat{p}_{\perp s}$) and they are given in the form of

$$\frac{\partial \delta\hat{n}_s}{\partial t} = \hat{u}_{\|c} + \varepsilon\hat{u}_{\|0} + (k_r \rho_{ti} q)\left[\delta\hat{p}_{\|0} + \delta\hat{p}_{\perp 0} + 2\hat{\phi}_0\right], \quad (B10)$$

$$\frac{\partial \hat{u}_{\|c}}{\partial t} = -\frac{q}{\varepsilon}\hat{u}_E \hat{S}_c - \delta\hat{p}_{\|s} - \hat{\phi}_s, \quad (B11)$$

$$\frac{\partial \delta\hat{n}_0}{\partial t} = \frac{\varepsilon}{2}\hat{u}_{\|s} + i\frac{(k_r \rho_{ti} q)}{2}\left[\delta\hat{p}_{\|s} + \delta\hat{p}_{\perp s} + 2\hat{\phi}_s\right], \quad (B12)$$

$$\frac{\partial \delta\hat{p}_{\|s}}{\partial t} = \left(\hat{q}_{\|c} + 3\hat{u}_{\|c}\right) - \varepsilon\left(2\hat{q}_{\perp 0} - \hat{q}_{\|0} - \hat{u}_{\|0}\right) + i(k_r \rho_{ti} q)\left[\delta\hat{r}_{\|\|0} + \delta\hat{r}_{\perp\|0} + 4\hat{\phi}_0\right], \quad (B13)$$

$$\frac{\partial \delta\hat{p}_{\perp s}}{\partial t} = \left(\hat{q}_{\perp c} + \hat{u}_{\|c}\right) + 2\varepsilon\left(\hat{q}_{\perp 0} + \hat{u}_{\|0}\right) + i(k_r \rho_{ti} q)\left[\delta\hat{r}_{\|\perp 0} + \delta\hat{r}_{\perp\perp 0} + 3\hat{\phi}_0\right]. \quad (B14)$$

To obtain linearized equations of Eqs. (B10)–(B14), we replace $\partial/\partial t$ with $-i\omega$ and replace higher order variables with lower order ones using closure relations shown in Eqs. (17) and (18). Then, the linearized equations for perturbed quantities can be represented by a simple matrix equation, which is given in the form of

$$\mathbf{M} \cdot \vec{x} = \begin{bmatrix} -i\omega & -1 & -2q & 0 & 0 \\ \tau_e & -i\omega & \frac{q}{\varepsilon}\tilde{S}_c & 1 & 0 \\ \tau_e q & 0 & -i\omega & q/2 & q/2 \\ -2\chi & -3 & -4q & -i\omega + 2\chi & 0 \\ -\chi & -1 & -3q & 0 & -i\omega + \chi \end{bmatrix} \begin{bmatrix} \delta\hat{n}_s \\ \hat{u}_{\|c} \\ \hat{u}_E \\ \delta\hat{p}_{\|s} \\ \delta\hat{p}_{\perp s} \end{bmatrix}$$

$$= \begin{bmatrix} 0 \\ 0 \\ 0 \\ 0 \\ 0 \end{bmatrix}. \quad (B15)$$

Then, one can finally derive a dispersion relation from Eq. (B15), giving rise to

$$\det|\mathbf{M}| = c_5\hat{\omega}^5 + c_4\hat{\omega}^4 + c_3\hat{\omega}^3 + c_2\hat{\omega}^2 + c_1\hat{\omega}^1 + c_0 = 0, \quad (B16)$$

where

$$c_5 = (-i)^5, \quad c_4 = (-i)^4[3\chi],$$

$$c_3 = (-i)^3\left[q^2\left(\frac{7}{2} + 2\tau_e\right) + 3 + \tau_e + 2\chi^2\right],$$

$$c_2 = (-i)^2\left[q^2\left\{2\chi(4 + 3\tau_e) - (2 + \tau_e)\frac{\hat{S}_c}{\varepsilon}\right\} + \chi(5 + 3\tau_e)\right],$$

$$c_1 = (-i)^1\left[q^2\left(\frac{5 + 3\tau_e}{2} + 4\chi^2(1 + \tau_e) - \chi(4 + 3\tau_e)\frac{\hat{S}_c}{\varepsilon}\right) + 2\chi^2(1 + \tau_e)\right], \quad (B17)$$

$$c_0 = (-i)^0\left[2q^2\chi(1 + \tau_e)\left(1 - \chi\frac{\hat{S}_c}{\varepsilon}\right)\right].$$

Note that, if there is no poloidal source ($\hat{S}_c = 0$), the coefficients shown in Eq. (B17) are exactly reduced to Eq. (D4) of Ref. 25 whose coefficients represent those of a fluid GAM dispersion relation. By solving Eq. (B16), one can find the source-driven modes can be excited only when the poloidal source is intense enough for the wave to overcome Landau damping.

APPENDIX C: EQUIVALENCE BETWEEN RMHD AND GLF4M MODELS

Here, we demonstrate the equivalence between the quasineutrality condition shown in Eq. (16) from the GLF4M model and the vorticity Eq. (8) from the rMHD model, in certain limits. From the quasi-neutrality condition in the GLF model, one can relate the ion polarization density to the continuity equation shown in Eq. (15a). The radial magnetic drift in the continuity equation of the GLF model explicitly provides the equivalence to the vorticity equation of the rMHD model. First, $\mathbf{E} \times \mathbf{B}$ flow is assumed to have only $m = 0$ component, giving the zero adiabatic electron density, $\delta n_{e_{\mathbf{k}_\perp}}/n_0 = \phi_{\mathbf{k}_\perp} - \langle\phi_{\mathbf{k}_\perp}\rangle_\psi = 0$. Then, the quasi-neutrality condition results in $\delta n_{i_{k,0}}/n_0 = -(ik_r \rho_{ti})^2 e\phi_{k,0}/T$. Keeping that condition, we obtain a vorticity equation

$$\frac{d\delta n_{i_{\mathbf{k}_\perp}}}{dt} + \mathbf{B} \cdot \nabla\frac{J_\|/e}{B} + 2i\omega_D \delta n_{i_{\mathbf{k}_\perp}} = 0 \quad (C1)$$

by multiplying the ionic charge number Z_s on Eq. (15a) and summing over species. Here, $J_\| = n_0 e(u_{i\|_{\mathbf{k}_\perp}} - u_{e\|_{\mathbf{k}_\perp}})$ is a parallel current density and the particle source for electrons and ions are same to satisfy the quasi-neutrality. The isotropic temperature $T_\perp = T_\|$ and the isothermal plasmas between species $T_i = T_e$ are assumed in the drift term.

Then, taking a flux-surface average on Eq. (C1) with a substitution of the quasi-neutrality condition of $\delta n_{i_{\mathbf{k}_r}}/n_0 = -(ik_r \rho_{ti})^2 e\phi_{\mathbf{k}_r}/T$ and the drift frequency of $i\omega_D = -(ik_r v_{Ti}^2/\Omega R)\sin\theta$ gives

$$\frac{\partial\langle u_E\rangle_\psi}{\partial t} = -\frac{2\varepsilon v_{Ti}^2}{r}\left\langle\frac{\delta n_{i_{\mathbf{k}_\perp}}}{n_0}\sin\theta\right\rangle_\psi. \quad (C2)$$

One can easily find that Eq. (C2) has exactly the same from as the vorticity Eq. (8) of the rMHD model.

APPENDIX D: MODIFIED PLASMA DISPERSION FUNCTION FOR GK DISPERSION RELATION

In this appendix, the definition of the modified dispersion relation Z_n used in Sec. IV is provided. We newly define

$$Z_n(\zeta) = \frac{1}{\sqrt{\pi}} \int_{-\infty}^{\infty} dt \, \frac{t^n \exp(-t^2)}{t - \zeta} \tag{D1}$$

for a simple representation of the GK dispersion relation presented in Eq. (27). Here, "n" is an arbitrary integer and Z_0 denotes the conventional plasma dispersion function. Then, Z_n can be derived by a combination of Z_0 and ζ whose from is given by

$$Z_n(\zeta) = \begin{cases} \zeta^n Z_0(\zeta) + \dfrac{1}{\sqrt{\pi}} \displaystyle\sum_{k=0}^{Q_2^{-(n+2)}} \Gamma\left(-\dfrac{2k+1}{2}\right) \zeta^{n+1+2k}, & n < -1, \\[2ex] \zeta^n Z_0(\zeta), & n = -1, 0, \\[1ex] \zeta^n Z_0(\zeta) + \zeta^{n-1}, & n = 1, 2, \\[1ex] \zeta^n Z_0(\zeta) + \zeta^{n-1} + \dfrac{1}{2} \displaystyle\sum_{k=0}^{Q_2^{n-3}} \dfrac{(2k+1)!}{4^k k!} a^{n-3-2k}, & n \geq 3, \end{cases} \tag{D2}$$

where Q_j^i means the quotient of i divided by j. Although our dispersion relation is somewhat simplified by considering only the resonance at $v_\parallel = qR_0$ and neglecting $\phi_{k_r,m}$ with $m \geq 2$, using Z_n will be more convenient if it involves more complicated physics, such as harmonic resonance occurring at $v_\parallel = n\,qR_0$ with $n \geq 2$ including $\phi_{k_r,m}$ with $m \geq 2$.

REFERENCES

[1]S. L. Milora, C. A. Foster, C. E. Thomas, C. E. Bush, J. B. Wilgen, E. A. Lazarus, J. L. Dunlap, P. H. Edmonds, W. A. Houlberg, H. C. Howe *et al.*, "Results of hydrogen pellet injection into ISX-B," Nucl. Fusion **20**, 1491 (1980).

[2]R. D. Durst, W. L. Rowan, M. E. Austin, R. A. Collins, R. F. Gandy, P. E. Phillips, and B. Richards, "Experimental observations of the dynamics of pellet ablation on the Texas Experimental Tokamak (TEXT)," Nucl. Fusion **30**, 3 (1990).

[3]L. R. Baylor, T. C. Jernigan, S. K. Combs, W. A. Houlberg, M. Murakami, P. Gohil, K. H. Burrell, C. M. Greenfield, R. J. Groebner, C.-L. Hsieh *et al.*, "Improved core fueling with high field side pellet injection in the DIII-D tokamak," Phys. Plasmas **7**, 1878 (2000).

[4]P. T. Lang, G. D. Conway, T. Eich, L. Fattorini, O. Gruber, S. Günter, L. D. Horton, S. Kalvin, A. Kallenbach, M. Kaufmann *et al.*, "ELM pace making and mitigation by pellet injection in ASDEX Upgrade," Nucl. Fusion **44**, 665 (2004).

[5]B. Pégourié, F. Köchl, H. Nehme, and A. R. Polevoi, "Recent results on the fuelling and control of plasmas by pellet injection, application to ITER," Plasma Phys. Controlled Fusion **51**, 124023 (2009).

[6]A. B. Hassam, T. M. Antonsen, Jr., J. F. Drake, and C. S. Liu, "Spontaneous poloidal spin-up of tokamaks and the transition to the H mode," Phys. Rev. Lett. **66**, 309 (1991).

[7]T. E. Stringer, "Diffusion in toroidal plasmas with radial electric field," Phys. Rev. Lett. **22**, 770 (1969).

[8]A. B. Hassam and J. F. Drake, "Spontaneous poloidal spin-up of tokamak plasmas: Reduced equations, physical mechanism, and sonic regimes," Phys. Fluids B **5**, 4022 (1993).

[9]P. Smeulders, L. C. Appel, B. Balet, T. C. Hender, L. Lauro-Taroni, D. Stork, B. Wolle, S. Ali-Arshad, B. Alper, H. J. De Blank *et al.*, "Survey of pellet enhanced performance in JET discharges," Nucl. Fusion **35**, 225 (1995).

[10]N. Winsor, J. L. Johnson, and J. M. Dawson, "Geodesic acoustic waves in hydromagnetic systems," Phys. Fluids **11**, 2448 (1968).

[11]K. Hallatschek and D. Biskamp, "Transport control by coherent zonal flows in the core/edge transitional regime," Phys. Rev. Lett. **86**, 1223 (2001).

[12]K. Itoh, K. Hallatschek, and S. I. Itoh, "Excitation of geodesic acoustic mode in toroidal plasmas," Plasma Phys. Controlled Fusion **47**, 451 (2005).

[13]N. Miyato, Y. Kishimoto, and J. Li, "Global structure of zonal flow and electromagnetic ion temperature gradient driven turbulence in tokamak plasmas," Phys. Plasmas **11**, 5557 (2004).

[14]N. Chakrabarti, R. Singh, P. K. Kaw, and P. N. Guzdar, "Nonlinear excitation of geodesic acoustic modes by drift waves," Phys. Plasmas **14**, 052308 (2007).

[15]H. Jhang, H. H. Kaang, S. S. Kim, T. Rhee, R. Singh, and T. S. Hahm, "Impact of zonal flows on edge pedestal collapse," Nucl. Fusion **57**, 022006 (2016).

[16]F. Zonca and L. Chen, "Radial structures and nonlinear excitation of geodesic acoustic modes," Europhys. Lett. **83**, 35001 (2008).

[17]Z. Qiu, L. Chen, and F. Zonca, "Excitation of kinetic geodesic acoustic modes by drift waves in nonuniform plasmas," Phys. Plasmas **21**, 022304 (2014).

[18]M. N. Rosenbluth, P. H. Rutherford, J. B. Taylor, E. A. Frieman, and L. M. Kovrizhnikh, "Neoclassical effects on plasma equilibria and rotation," in *Proceedings of the Fourth International Conference on Plasma Physics and Controlled Nuclear Fusion Research* (IAEA, Vienna, 1971), Vol. 1.

[19]T. H. Stix, "Decay of poloidal rotation in a tokamak plasma," Phys. Fluids **16**, 1260 (1973).

[20]M. N. Rosenbluth and F. L. Hinton, "Poloidal flow driven by ion-temperature-gradient turbulence in tokamaks," Phys. Rev. Lett. **80**, 724 (1998).

[21]V. B. Lebedev, P. N. Yushmanov, P. H. Diamond, S. V. Novakovskii, and A. I. Smolyakov, "Plateau regime dynamics of the relaxation of poloidal rotation in tokamak plasmas," Phys. Plasmas **3**, 3023 (1996).

[22]H. Sugama and T.-H. Watanabe, "Collisionless damping of geodesic acoustic modes," J. Plasma Phys. **72**, 825 (2006).

[23]Z. Gao, K. Itoh, H. Sanuki, and J. Q. Dong, "Eigenmode analysis of geodesic acoustic modes," Phys. Plasmas **15**, 072511 (2008).

[24]G. W. Hammett and F. W. Perkins, "Fluid moment models for Landau damping with application to the ion-temperature-gradient instability," Phys. Rev. Lett. **64**, 3019 (1990).

[25]H. Sugama, T.-H. Watanabe, and W. Horton, "Collisionless kinetic-fluid model of zonal flows in toroidal plasmas," Phys. Plasmas **14**, 022502 (2007).

[26]F. L. Hinton and M. N. Rosenbluth, "Dynamics of axisymmetric and poloidal flows in tokamaks," Plasma Phys. Controlled Fusion **41**, A653 (1999).

[27]W. Dorland and G. W. Hammett, "Gyrofluid turbulence models with kinetic effects," Phys. Fluids B **5**, 812 (1993).

[28]M. A. Beer, "Gyrofluid models of turbulent transport in tokamaks," Ph.D. thesis (Princeton University, 1995).

[29]M. A. Beer and G. W. Hammett, "Toroidal gyrofluid equations for simulations of tokamak turbulence," Phys. Plasmas **3**, 4046 (1996).

[30]M. Valovič, K. Axon, L. Garzotti, S. Saarelma, A. Thyagaraja, R. Akers, C. Gurl, A. Kirk, B. Lloyd, G. P. Maddison *et al.*, "Particle confinement of pellet-fuelled tokamak plasma," Nucl. Fusion **48**, 075006 (2008).